

RESEARCH

Open Access



A Stepwise decision tree model for differential diagnosis of Kimura's disease in the head and neck

Rui Luo^{1†}, Gongxin Yang^{1†}, Huimin Shi¹, Yining He², Yongshun Han¹, Zhen Tian³ and Yingwei Wu^{1*}

Abstract

Objectives This study aims to differentiate Kimura's disease (KD) from Sjogren's syndrome with mucosa-associated lymphoid tissue lymphoma (SS&MALT), neurofibromatosis (NF), and lymphoma in the head and neck by using a stepwise decision tree approach.

Materials and methods A retrospective analysis of 202 patients with pathologically confirmed KD, SS&MALT, NF, or lymphoma was conducted. Demographic and magnetic resonance imaging (MRI) data were collected, with qualitative features (e.g., skin thickening, lesion morphology, lymphadenopathy, MRI signal intensity) and quantitative variables (e.g., age, lesion size, apparent diffusion coefficients (ADCs), wash-in rate, time to peak (TTP), time-signal intensity curve (TIC) patterns) examined. A stepwise decision-tree model using the classification and regression trees (CART) algorithm was developed to aid in the differential diagnosis of KD in the head and neck. The model's diagnostic accuracy and misclassification risk were assessed to evaluate its reliability and effectiveness.

Results Key characteristics for KD included male predominance (91.7%), frequent lymphadenopathy (86.1%), and skin thickening (72.2%). Primary lesions of NF typically exhibited higher ADCs compared to those of KD, SS&MALT, and lymphoma. In lymphadenopathy, however, unique ADC patterns were observed: in KD, the ADCs of lymphadenopathy were lower than those of primary lesions, whereas in lymphoma, the ADCs of lymphadenopathy were comparable to those of primary lesions. Predictors for distinguishing KD included lesion's location, ADCs, lymphadenopathy, and sizes (all $p < 0.001$). The decision-tree model achieved an impressive 99.0% accuracy in the differential diagnosis across the overall cohort, with a 10-fold cross-validated misclassification risk of 0.079 ± 0.024 .

Conclusion The stepwise decision tree model, based on MRI features, showed high accuracy in differentiating KD from other head and neck diseases, offering a reliable diagnostic tool in clinical practice.

Clinical relevance KD is characterized by male predominance, skin thickening, and high incidence of lymphadenopathy. ADCs and TIC patterns are distinguishable in differentiating KD from SS&MALT, NF, and lymphoma in the head and neck. The decision tree model enhances the understanding of KD imaging features and facilitates

[†]Rui Luo and Gongxin Yang contributed equally to this work.

*Correspondence:
Yingwei Wu
wuyw0103@hotmail.com

Full list of author information is available at the end of the article



accurate KD diagnosis, offering an easily accessible and convenient diagnostic tool for radiologists and physicians in daily practice and guiding tailored clinical management plans for affected patients.

Clinical trial number Not applicable.

Key points

- KD is characterized by male predominance, skin thickening, and a high incidence of lymphadenopathy.
- Multiple lesions with varying morphological patterns are commonly seen in KD.
- ADCs and TIC patterns are useful for differentiating KD from SS&MALT, NF and lymphoma in the head and neck.
- A stepwise decision tree model, based on MRI variables, aids in the differential diagnosis of KD and other head and neck diseases, providing a convenient and accessible diagnostic tool for radiologists and physicians in daily practice.

Keywords KD, Head and neck diseases, MRI, Lymphadenopathy, Decision tree

Introduction

KD, a rare chronic immune disease with an incidence of less than 1/100,000 [1], was first reported by Kim and Szeto in 1937 [2] and further described by Kimura in 1948 [3]. KD primarily affects young males of Asian lineage [4]. To date, there have been about 300 reported cases globally; however, the largest reported KD patient cohort consisted of 52 cases from PubMed [5].

Clinically, KD typically presents as a slow, progressive condition, with symptoms lasting on average of 4 years before diagnosis [6]. The manifestations of KD may vary, including subcutaneous mass-like lesions in the head and neck region as well as painless swelling in the major salivary glands with local lymphadenopathy. While KD predominantly affects the head and neck, it can also involve other organs, such as the eyes and kidneys. Patients with KD often show increased peripheral eosinophil counts (5.8–51%) and elevated serum IgE levels (193–6827 U/mL) [5, 7–9]. Histologically, KD is characterized by chronic inflammation, with significant eosinophilic infiltration, variable vascular proliferation, and fibrosis [7]. Though the exact cause of KD remains unknown, it has been thought to be an autoimmune reaction, possibly triggered by external stimuli. The involvement of IgE-mediated type 1 hypersensitivity and Th2-driven immune responses suggests a link to allergic reactions, explaining the disease's eosinophil-rich inflammation [8, 10–12].

Routine radiologic findings in KD are often nonspecific and can overlap with those of other head and neck conditions [4, 13–16]. On MRI, KD typically appears as a hypo-intense lesion on T1-weighted images (T1WI) and may show varied signal intensities on T2-weighted images (T2WI). These variations in T2WI signal intensity are influenced by the degree of fibrosis and vascularity in the lesions. Fibrotic tissue generally results in lower signal intensity on T2WI, while increased vascularity corresponds to higher T2WI intensity [4, 14]. In addition, KD may present as poorly defined subcutaneous masses, enlarged salivary glands, and lymphadenopathy, which

can mimic other diseases like mucosa-associated lymphoid tissue lymphoma, primary lymphoma, or NF, all of which may present similarly on computed tomography (CT) or MRI [17–20]. Moreover, both KD and NF may exhibit skin thickening adjacent to the primary lesions, which can complicate differentiation between the two conditions [20–23]. Due to the relatively high recurrence rate of KD, its management can be complex, involving surgical excision, oral corticosteroids, systemic immunosuppressive medications, and in some cases, radiation therapy [6]. Therefore, accurate diagnosis is crucial to prevent unnecessary treatments and ensure effective management, ultimately improving patient outcomes of KD.

Given the relatively small number of KD cases in the database and its overlap in clinical and radiological features with other head and neck diseases, differentiating KD from other conditions is clinically challenging. In such cases, a decision tree model, particularly one based on the CART algorithm, offers significant advantages. The CART algorithm is well-suited for situations with limited data points, where decisions must be made based on complex, multifactorial features, such as radiological and clinical data [24, 25]. For KD, a disease with limited available cases, the CART model can still identify patterns by dividing the dataset into subsets based on key features, creating a tree-like structure that helps classify different diseases. For example, Vallee et al. utilized MRI data with the CART algorithm to classify intracranial lymphomas, glioblastomas, and metastatic tumors, also achieving 96% accuracy [26]. The efficiency and ease of interpretation of CART make it particularly useful for rare diseases like KD, where traditional diagnostic methods may struggle.

The purpose of this study is to evaluate and clarify the radiological features of KD, with a specific focus on distinguishing it from other head and neck conditions. We analysed 36 pathologically confirmed KD cases from a hospital database spanning 2009 to 2024, incorporating

both routine and functional MRI data. To enhance diagnostic accuracy and ease, we applied a CART-based decision tree model to differentiate KD from other similar head and neck diseases, providing a practical tool for both radiologists and clinicians.

Materials and methods

Patient selection

This study was conducted in accordance with the Declaration of Helsinki and was approved by the Medical Ethics Committee of Shanghai Ninth People's Hospital, Shanghai Jiao Tong University School of Medicine (No. SH9H-2024-T168-1). Patients with pathologically confirmed KD, SS&MALT, NF or lymphoma were consecutively included between 2009 and 2024 at Shanghai Ninth People's Hospital of Shanghai Jiao Tong University School of Medicine. The patient selection criteria were as follows:

1. All patients were pathologically diagnosed with KD, SS&MALT, NF or lymphoma.
2. Head and neck lesions involving subcutaneous tissue, glands and/or cervical lymphadenopathy were observed for each patient.
3. MRI data were completely available for each patient, and the image quality was favourable for analysis.

And the patient exclusion criteria were as follows:

1. Lesions were not located in the head and neck.
2. Preoperative MRI was not performed.
3. DWI or dynamic contrast-enhanced MRI (DCE-MRI) was not available.
4. Artifacts affected imaging analysis (See Fig. 1).

MR image acquisition

Of all 202 subjects, 22 were scanned on 1.5T MRI (GE Signa Twinspeed USA); 180 were scanned on 3.0T MRI (Philips Ingenia 3.0T Netherlands). Axial T1WI, T2WI

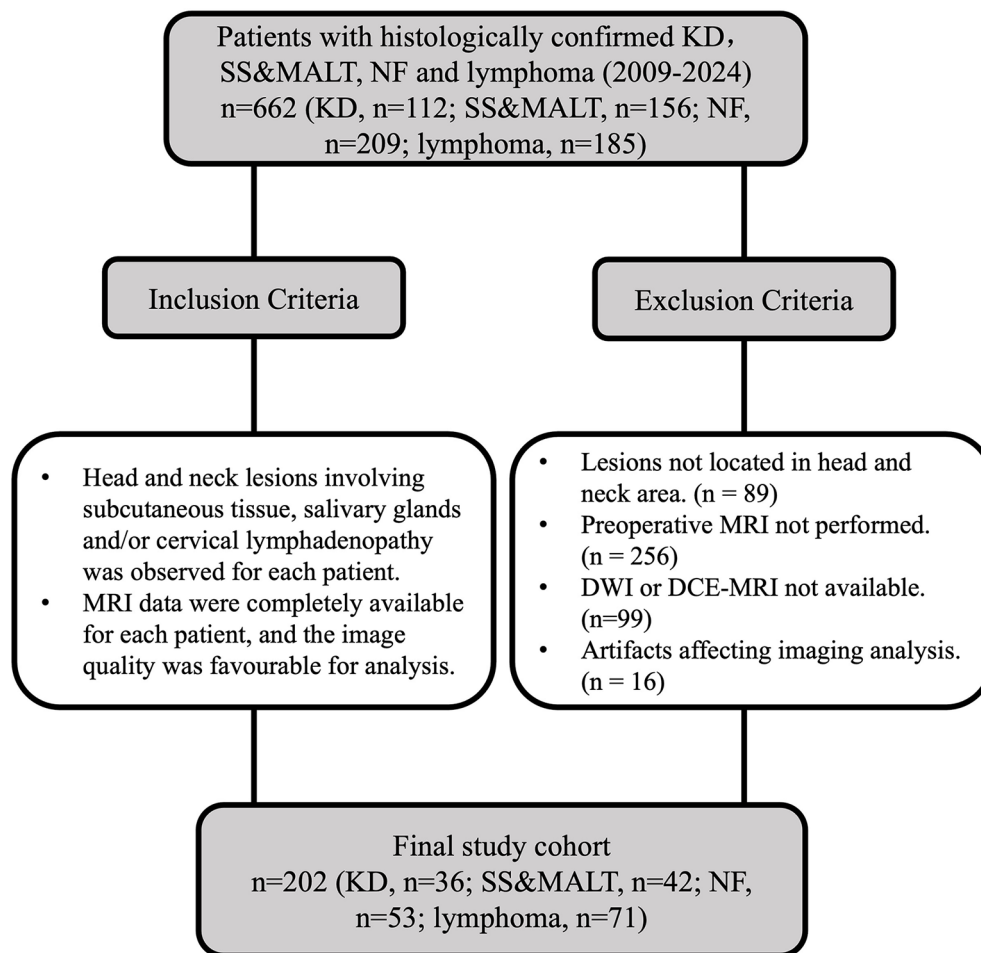


Fig. 1 Flowchart of study patients with selected head and neck diseases. Flowchart outlined the selection process for patients diagnosed with KD, SS&MALT, NF and primary lymphoma. The chart detailed the inclusion and exclusion criteria leading to the final patient cohorts used in the study. Abbreviations: KD, Kimura's disease; SS&MALT, Sjogren's syndrome with mucosa-associated lymphoid tissue lymphoma; NF, neurofibromatosis

or fat-suppressed T2WI on axial and coronal images and DWI (b value, 1000 s/mm²) were performed in the same transverse plane. After contrast injection, axial fat-suppressed and contrast-enhanced T1WI and DCE-MRI were acquired. The specific scanning parameters are shown in Table 1.

Image post-processing and data analysis

All images were reviewed by two senior radiologists. For primary lesions involving subcutaneous tissue or glands in the head and neck region, the lesion's location, distribution, number, size, shape, and adjacent skin thickening were recorded and measured. Skin thickening was defined as a para-lesion skin thickness to contralateral normal skin thickness ratio of $\geq 1.2:1$. Lymphadenopathy was identified when cervical lymph nodes in levels I and II were > 15 mm in length, levels III-VII were > 10 mm, and lymph nodes in the salivary glands were > 8 mm. Clustered changes in lymphadenopathy were defined as involvement of three or more lymph nodes within the typical drainage area of the lesion [27].

The raw DWI and DCE-MRI data were processed offline on a workstation (AMAX, TS40-X2, China) using the Philips IntelliSpace Portal software. ADC maps and TICs were subsequently obtained. Regions of interest (ROIs) were manually outlined by two experienced radiologists based on fat-suppressed and contrast-enhanced T1WI, ensuring inclusion of the entire lesion while excluding obvious necrotic and cystic areas. For ADC measurement, ROIs were placed on all slices showing lesions or lymphadenopathy, and the average ADC value

was calculated. To minimize bias, lymph nodes smaller than 1 cm were excluded from ADC measurement.

TICs were categorized into four patterns (types I-IV) based on wash-out rates and time to peak (TTP) [14]:

- Type I: TTP > 120 s.
- Type II: TTP ≤ 120 s with a wash-out rate $\leq 30\%$.
- Type III: TTP ≤ 120 s with a wash-out rate $> 30\%$.
- Type IV: no enhancement.

The Stepwise decision-tree model

A stepwise decision-tree model was developed to differentiate KD from three other similar conditions using the CART algorithm. The CART method splits data into two child nodes at each step, aiming to create more homogeneous subgroups based on optimal split points selected through criteria like the Gini index or information gain. This iterative splitting process constructs the decision tree and generates prediction rules to classify the data accurately [26].

To minimize the risk of overfitting, several strategies were employed. First, k-fold cross-validation was implemented to further validate the model's performance. The dataset was divided into 10 mutually exclusive subsets, or "folds," of roughly equal size (with $k = 10$ in this study). During each iteration of cross-validation, the model was trained on 9 folds and tested on the remaining fold, rotating through all folds. After evaluating the results of the 10-fold cross-validation, the decision tree model was pruned by adjusting the minimum sample size of the parent nodes and child nodes. The values for the minimum sample size were chosen based on a balance between

Table 1 Model of MRI machine and detailed parameters of each scanning sequence

Sequences	FOV (mm ²)	FA (°)	TR/TE (ms/ms)	Slice thickness (mm)	Slice gap (mm)	Matrix size	Contrast administration
Signa 1.5T Twinspeed							
T1WI(FSE)	240*240	90	540/9	5	6	512*512	
T2WI(FSFSE)	240*240	90	4440/94	5	6	512*512	
T2WI-Cor(FSE)	220*220	90	3700/80	4	5	512*512	
DWI(SE-EPI)	240*240	90	2200/70	5	5.5	256*256	
T1WI + C(FSFSE)	240*240	90	700/9	5	6	512*512	
T1WI + C-Cor(FSFSE)	220*220	90	500/10	4	5	512*512	
DCE-MRI(FSPGR)	240*240	30	4/2	5	5.5	256*256	15 ml Gd-DT-PA at 3.0 ml/s
Ingenia 3.0T							
T1WI(TSE)	210*210	90	641/18	4	4.5	512*512	
T2WI (HR-mDIXON-TSE-RL)	210*210	90	2810/85	4	4.5	384*384	
T2WI-Cor (SS-mDIXON)	210*210	90	3000/80	3	3.3	864*864	
DWI(SPAIR)	222*222	90	2254/68	5	5.5	192*192	
T1WI + C (mDIXON-TSE-Fast)	209*209	90	582/15	4	4.5	336*336	
T1WI + C-Cor (mDIXON-TSE-FH)	210*210	90	589/16	3	3.3	432*432	
DCE-MRI(THRIVE)	210*210	10	7/4	6	3	320*320	15 ml Gd-DT-PA at 3.0 ml/s

model complexity and generalization ability [28]. In this study, the minimum sample size for parent nodes and child nodes was set to 5 and 2, respectively. The maximum depth of the decision tree was set to 3. This pruning approach allowed for a robust assessment of the model's ability to generalize to new data, preventing overfitting while retaining model accuracy. Finally, the model's performance was evaluated based on two metrics: the overall accuracy and the classification accuracy for each of the four diseases. The cross-validated estimates were calculated as the average accuracy scores from each of the 10 test folds, providing an estimate of the model's predictive reliability across different subsets of the data.

Statistical analysis

Statistical analyses were performed using IBM SPSS Statistics (version 26.0). Continuous variables were expressed as the mean \pm standard deviation and compared by independent t tests, Mann-Whitney U or Kruskal-Wallis H test. Categorical variables were presented as numbers and percentages and were compared by the Chi-square test or Fisher's exact test. $P < 0.05$ was considered statistically significant.

Results

Patient demographic characteristics

We reviewed the demographic characteristics of 202 patients with specific diseases. As shown in Table 2, the median age of onset for NF, KD, SS&MALT, and lymphoma was 22.5 (15.5, 29.0), 37.0 (19.0, 49.8), 49.5 (37.0, 65.3), and 60.5 (52.5, 68.0) years, respectively. KD was more common in males (91.7%), whereas SS&MALT was predominantly seen in females (90.5%). No significant sex differences were observed for lymphoma or NF. The location and distribution of primary lesions in KD showed similarities to those in NF, SS&MALT, and lymphoma, but were not entirely identical. KD and NF commonly involved subcutaneous tissue in the head and neck area, and larger lesions occasionally affected both the glands (lacrimonal or salivary glands) and subcutaneous regions (16/31 for KD and 32/53 for NF). SS&MALT affected only the salivary glands, while lymphoma primarily involved submucosal and subcutaneous tissues, with rare salivary gland involvement. Bilateral lesions were common across all cases except for lymphoma, with the highest frequency of 64.3% in SS&MALT. The maximum diameter for primary lesions was significantly smaller in SS&MALT compared to KD (1.4 vs. 4.5 cm; $p < 0.001$),

Table 2 General characteristics of patients with KD and the other three head and neck conditions

Characteristics		KD (n = 36)	SS&MALT (n = 42)	NF (n = 53)	Lymphoma (n = 71)	p
Age (yrs)		37.0 (19.0,49.8)	49.5 (37.0,65.3)	22.5 (15.5,29.0)	60.5 (52.5,68.0)	< 0.001
Sex	Male	33 (91.7%)	4 (9.5%)	32 (60.4%)	47 (66.2%)	< 0.001
	Female	3 (8.3%)	38 (90.5%)	21 (39.6%)	24 (33.8%)	
*Primary lesions		n = 31	n = 42	n = 53	n = 47	
Location	*Gland and subcutaneous	16 (51.6%)	0	32 (60.4%)	0	< 0.001
	*Gland	3 (9.7%)	42 (100.0%)	0	5 (10.6%)	
	Subcutaneous	11 (35.5%)	0	21 (39.6%)	12 (25.5%)	
	Submucosa	1 (3.2%)	0	0	30 (63.8%)	
Unilateral		25 (80.6%)	15 (35.7%)	49 (92.5%)	47 (100.0%)	< 0.001
Bilateral		6 (19.4%)	27 (64.3%)	4 (7.5%)	0	
Number	Single	21 (67.7%)	7 (16.7%)	49 (92.5%)	45 (95.7%)	< 0.001
	Multiple	10 (32.3%)	35 (83.3%)	4 (7.5%)	2 (4.3%)	
maximum diameter (cm)		4.5 (3.6,5.7)	1.4 (0.9,1.9)	10.4 (5.0,14.2)	3.6 (2.4,6.5)	< 0.001
Lymphadenopathy		n = 31			n = 45	
Location	Cervical and parotid	11 (35.5%)			3 (6.7%)	< 0.001
	Cervical	6 (19.4%)			40 (88.9%)	
	parotid	14 (45.2%)			2 (4.4%)	
Unilateral		6 (19.4%)			33 (73.3%)	< 0.001
Bilateral		25 (80.6%)			12 (26.7%)	
Number	Single	11 (35.5%)			19 (42.2%)	0.636
	Multiple	20 (64.5%)			26 (57.8%)	
maximum diameter (cm)		1.6 (1.2,2.0)			2.0 (1.6,2.5)	< 0.001

*Primary lesions: extra-nodal soft tissue lesions

*Gland: parotid and lacrimonal gland. Abbreviations: KD: Kimura's disease, SS&MALT: Sjogren's syndrome with mucosa-associated lymphoid tissue lymphoma, NF: neurofibromatosis

NF (1.4 vs. 10.4 cm; $p < 0.001$), and primary lymphoma (1.4 vs. 3.6 cm; $p < 0.01$). Lymphadenopathy was more frequently observed in KD (86.1%) than in lymphoma (63.4%), though lymph nodes were larger in lymphoma, with a maximum diameter of 2.0 cm compared to 1.6 cm in KD ($p < 0.001$).

Characteristics on routine MRI

Primary lesions across the four diseases generally appeared iso-intense on T1WI and hyper-intense on fat-suppressed T2WI, with most showing strong enhancement after contrast administration (Table 3). In KD, 93.5% of primary lesions displayed heterogeneous enhancement (Fig. 2), while 89.4% of lymphoma lesions showed homogeneous enhancement. Skin thickening was found as a distinctive feature in KD and NF, occurring at significantly higher frequency (72.2% in KD and 94.3% in NF; both $p < 0.001$) compared to lymphoma (1.4%) and SS&MALT (0%) (Table 3). Lymphadenopathy was prominent in KD (86.1%) and lymphoma (63.4%) but

absent in SS&MALT and NF (Table 3; Figs. 3 and 4). In KD, while primary lesions often showed heterogeneous enhancement, all associated lymphadenopathy exhibited a mild to marked homogeneous enhancement pattern. In contrast, 31.1% of lymphoma cases showed heterogeneous enhancement in lymphadenopathy.

Characteristics on functional MRI

We analyzed TIC patterns from DCE-MRI and ADCs from DWI to differentiate among the four diseases. As shown in Table 4 and Figure 5, the primary lesions of NF had significantly higher ADCs than KD (1.58 vs. 1.04, $p < 0.05$), SS&MALT (1.58 vs. 0.63, $p < 0.001$), and lymphoma (1.58 vs. 0.67, $p < 0.001$). Additionally, ADCs differed significantly between KD and SS&MALT (1.04 vs. 0.63, $p < 0.001$) and between KD and lymphoma (1.04 vs. 0.67, $p < 0.01$). In KD, lymphadenopathy had lower ADCs than primary lesions (0.67 vs. 1.04), while in lymphoma, ADCs were similar between lymphadenopathy and primary lesions (0.67 vs. 0.58). In addition, for cases of KD

Table 3 Routine MRI characteristics across four head and neck conditions

Characteristics		KD (n = 36)	SS&MALT (n = 42)	NF (n = 53)	Lymphoma (n = 71)	p
*Skin thickening		26 (72.2%)	0	50 (94.3%)	1 (1.4%)	< 0.001
Lymphadenopathy		31 (86.1%)	0	0	45 (63.4%)	< 0.001
*Cluster		10 (27.8%)			24 (33.8%)	0.661
*Primary lesions		n = 31	n = 42	n = 53	n = 47	
T1WI	Isointense	31 (100.0%)	42 (100.0%)	53 (100.0%)	47 (100.0%)	
T2WI	Hyperintense	31 (100.0%)	42 (100.0%)	53 (100.0%)	47 (100.0%)	
Enhancement	Homogeneous, marked	2 (6.5%)	11 (26.2%)	18 (34.0%)	40 (85.1%)	< 0.001
	Heterogeneous, marked	28 (90.3%)	31 (73.8%)	35 (66.0%)	5 (10.6%)	
	Homogeneous, mild	0	0	0	2 (4.3%)	
	Heterogeneous, mild	1 (3.2%)	0	0	0	
Lymphadenopathy		n = 31			n = 45	
T1WI	Isointense	31 (100.0%)			45 (100.0%)	
T2WI	Hyperintense	31 (100.0%)			45 (100.0%)	
Enhancement	Homogeneous, marked	29 (93.5%)			31 (68.9%)	< 0.001
	Heterogeneous, marked	0			14 (31.1%)	
	Homogeneous, mild	2 (6.5%)			0	

*Skin thickening: a thickness ratio of para-lesion skin to contralateral normal skin $\geq 1.2:1$

*Cluster: three or more lymph nodes involved within the typical drainage area of the lesion

*Primary lesions: extra-nodal soft tissue lesions. *Abbreviations:* KD: Kimura's disease, SS&MALT: Sjogren's syndrome with mucosa-associated lymphoid tissue lymphoma, NF: neurofibromatosis

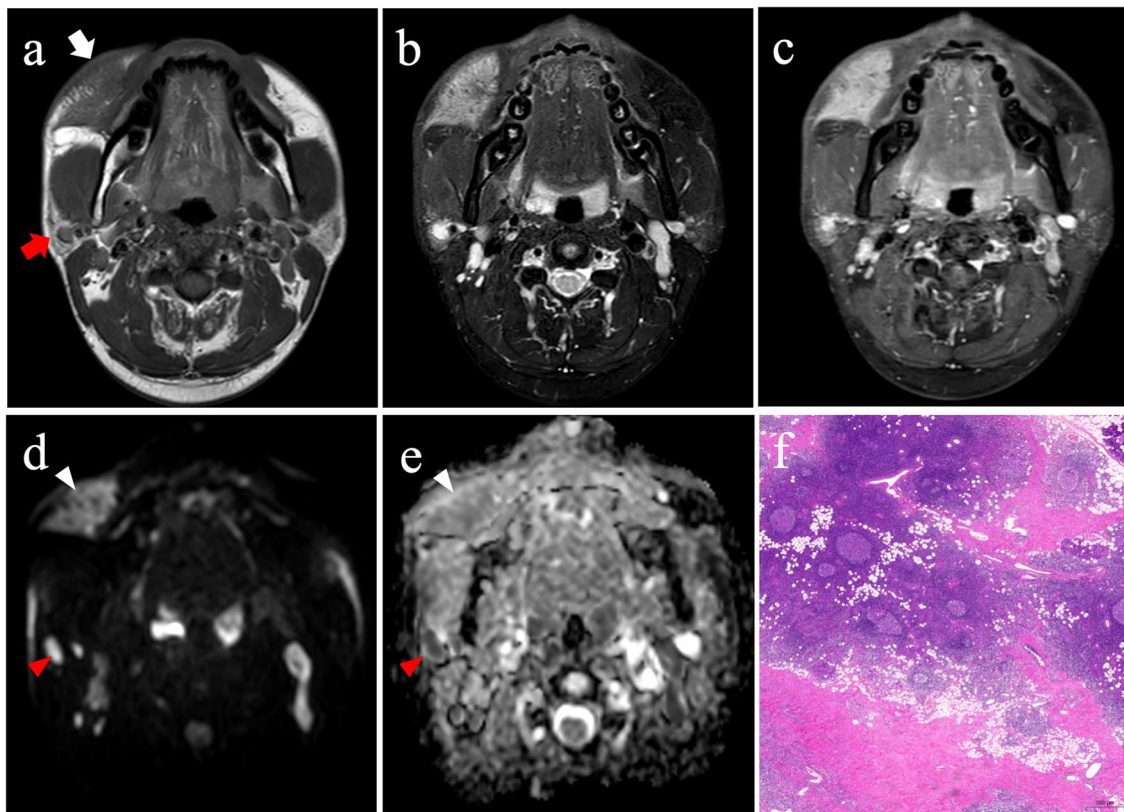


Fig. 2 Representative case of KD. Imaging and histopathological findings from a patient diagnosed with KD. (a) Axial T1WI and (b) fat-suppressed T2WI showed a well-defined subcutaneous lesion (white arrow) with adjacent skin thickening and right-sided parotid lymphadenopathy (red arrow). (c) Contrast-enhanced axial fat-suppressed T1WI demonstrated homogeneous enhancement of both the subcutaneous lesion and lymphadenopathy. (d) DWI revealed hyperintensity in both the subcutaneous lesion and lymphadenopathy, indicating restricted diffusion. (e) The ADC map showed higher ADCs in the subcutaneous lesion (white arrowhead) compared to the lymphadenopathy (red arrowhead). (f) Histological examination with haematoxylin-eosin (H&E) staining ($\times 20$ magnification) revealed hyperplastic lymphoid follicles with diffuse eosinophilic infiltration, consistent with a diagnosis of KD

and lymphoma with both primary lesions and lymphadenopathy, the ADC differences between primary lesions and lymphadenopathy (Δ ADC) demonstrated a strong diagnostic ability in differentiating KD from lymphoma, with values of 0.37 ± 0.21 vs. 0.11 ± 0.05 ($p < 0.001$). TIC patterns, classified into four types (I-IV), also helped distinguish disease types. Primary lesions of KD were mainly type I (51.6%) and type II (48.4%), similar to NF, which were 83.0% type I and 17.0% type II. Most SS&MALT primary lesions were type II (76.2%), while lymphoma primary lesions showed a broader range (types I-III). In lymphadenopathy, TIC patterns effectively differentiated KD (mainly type II, 89.3%) from lymphoma, which displayed a mix of types I-III. TTP for primary lesions was significantly longer in NF compared to SS&MALT (185.8 vs. 39.5; $p < 0.001$) and lymphoma (185.8 vs. 44.0; $p < 0.001$). Although TTP differences between KD and NF were not significant, KD showed a significantly longer TTP compared to SS&MALT (108.0 vs. 39.5; $p < 0.001$).

Stepwise classification of the decision tree model

Since a single imaging parameter was ineffective in differentiating KD from three other head and neck conditions, we adopted a stepwise approach for better discrimination. Key predictors identified for distinguishing KD included lesion's location, ADCs, lymphadenopathy, and maximum diameters, with a significance level of $p < 0.001$. As shown in Fig. 6, the ADC value of $0.83 \times 10^{-3} \text{ mm}^2/\text{s}$ was the first criterion for splitting. Higher ADCs were commonly associated with KD and NF, while lower ADCs were found in SS&MALT and primary lymphoma, except for 9 cases of KD (Fig. 6, left panel). Then, in the second tier, parotid gland involvement was a distinctive feature for SS&MALT, achieving 100% accuracy. For cases with lower ADCs but no parotid involvement, a maximum diameter of 2.2 cm in lymphadenopathy effectively distinguished KD from primary lymphoma, with 100% accuracy for KD (diameter ≤ 2.2 cm) and 98.4% for lymphoma (diameter > 2.2 cm). On the right panel, for cases with larger ADCs, the presence of lymphadenopathy was also a strong indicator of KD, achieving 100% accuracy. In contrast, for cases without lymphadenopathy, KD

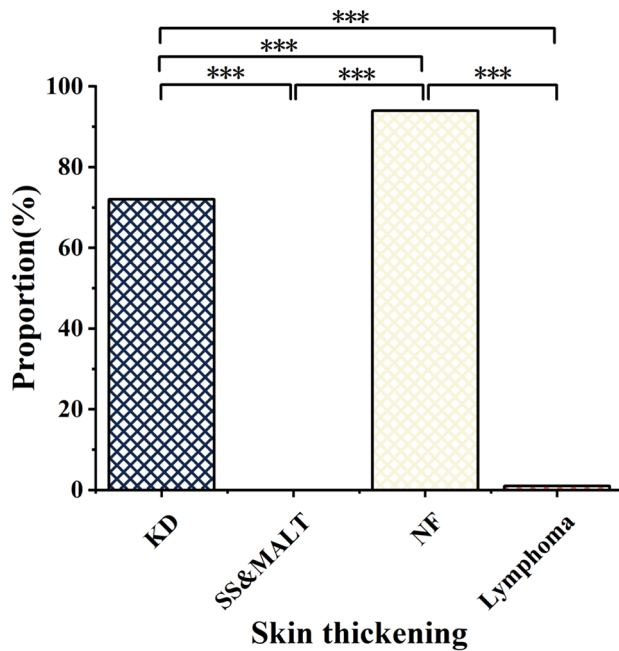


Fig. 3 Comparison of skin thickening frequency in KD and three other head and neck conditions. Significantly different P values at $P < 0.001$ (***), Chi-square test. Abbreviations: KD: Kimura's disease, SS&MALT: Sjogren's syndrome with mucosa-associated lymphoid tissue lymphoma, NF: neurofibromatosis

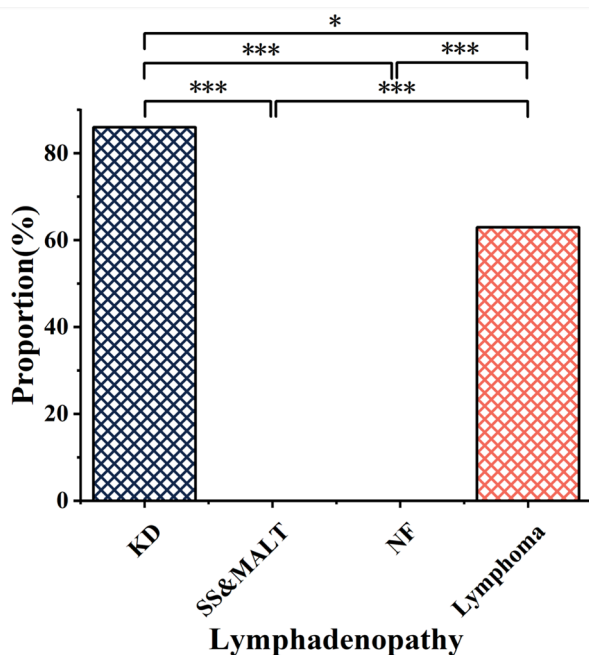


Fig. 4 Comparison of lymphadenopathy presence in KD and three other head and neck conditions. Significantly different P values at $P < 0.05$ (*) or $P < 0.001$ (***), Chi-square test. Abbreviations: KD: Kimura's disease, SS&MALT: Sjogren's syndrome with mucosa-associated lymphoid tissue lymphoma, NF: neurofibromatosis

was further differentiated from NF based on a higher ADC cut-off of $1.2 \times 10^{-3} \text{ mm}^2/\text{s}$, yielding 100% accuracy for KD ($\text{ADCs} \leq 1.2 \times 10^{-3} \text{ mm}^2/\text{s}$) and 98.1% for NF ($\text{ADCs} > 1.2 \times 10^{-3} \text{ mm}^2/\text{s}$). Overall, the stepwise decision tree model achieved an impressive accuracy of 99.0% in predicting these four diseases individually, with a misclassification risk of 0.079 ± 0.024 , as estimated by 10-fold cross-validation. Specifically, the classification accuracy for KD was 94.4%, while the accuracies for SS&MALT, NF and lymphoma were all 100%.

Two cases of KD were misclassified as lymphoma and NF, respectively. The primary reason for misclassifying the first case of KD as lymphoma was the presentation of markedly enlarged, bilateral lymph nodes across multiple cervical levels (II-V), including the parotid gland. The significant size of the largest lymph node (up to 6 cm) closely resembled the pattern seen in lymphoma. The second case of KD presented with a patchy primary lesion with ill-defined borders, involving both the left lacrimal gland and adjacent soft tissues. The ADCs, which were influenced by tissue characteristics such as cellularity and water content, were likely elevated in this case due to the lesion's soft tissue involvement. This elevated ADC further complicated the diagnosis and contributed to the misclassification as NF.

Discussion

Clinically, diagnosing KD can be challenging due to its nonspecific symptoms. Predominantly affecting males, young individuals (ages 10–40), and Asians, our study found a male predominance (91.7%) with a median age of 37 years, consistent with previous studies [4]. KD often presents with subcutaneous nodules or lesions in the head and neck, which resembles conditions such as parotid neoplasms, malignant lymphomas, or inflammatory diseases. Lymphadenopathy is a common feature of KD, with incidences ranging from 25 to 100% in the literature [4, 8, 15]. Our study observed a relatively high incidence of 86.1%. However, lymphadenopathy can be confused with conditions like Castleman's disease or Hodgkin's lymphoma, complicating the diagnostic process.

Imaging features of KD

While imaging alone could not confirm a KD diagnosis, both CT and MRI played vital roles in assessing the disease's extent and excluding other malignancies. There has been no consensus on specific imaging findings for KD, with reports showing both specific signal changes [4] and a lack of distinct features [8]. In our study, we observed two main morphological patterns in primary KD lesions: a well-defined nodular pattern and an ill-defined infiltrative pattern, which were sometimes present simultaneously (Fig. 7). On T1WI and T2WI, primary lesions and

Table 4 Functional MRI characteristics of KD and three other head and neck conditions

Characteristics	KD (n = 36)	SS&MALT (n = 42)	NF (n = 53)	Lymphoma (n = 71)	p
* Δ ADC ($\times 10^{-3}$ mm ² /s)	0.37 \pm 0.21			0.11 \pm 0.05	< 0.001
*Primary lesions					
*ADC ($\times 10^{-3}$ mm ² /s)	1.04 (0.95,1.26)	0.63 (0.56,0.69)	1.58 (1.44,1.76)	0.67 (0.58,0.76)	< 0.001
*TIC					
Type I	16 (51.6%)	0	44 (83.0%)	9 (20.0%)	< 0.001
Type II	15 (48.4%)	32 (76.2%)	9 (17.0%)	31 (68.9%)	
Type III	0	10 (23.8%)	0	5 (11.1%)	
Wash-in rate (s ⁻¹)	21.2 (5.9,52.5)	46.9 (27.4,58.1)	35.8 (17.8,48.5)	48.6 (24.9,65.5)	0.018
*TTP (s)	108.0 (50.0,177.0)	39.5 (35.5,53.2)	185.8 (116.8,199.5)	44.0 (38.5,68.0)	< 0.001
Lymphadenopathy					
*ADC ($\times 10^{-3}$ mm ² /s)	0.67 (0.61,0.76)			0.58 (0.52,0.62)	< 0.001
*TIC					
Type I	0			9 (21.4%)	0.013
Type II	25 (89.3%)			26 (61.9%)	
Type III	3 (10.7%)			7 (16.7%)	
Wash-in rate (s ⁻¹)	40.5 \pm 30.5			44.6 \pm 21.4	0.622
*TTP (s)	43.5 (34.2,56.6)			44.5 (35.0,71.8)	0.472

*Primary lesions: extra-nodal soft tissue lesions

*ADC: apparent diffusion coefficient

*TIC: time-signal intensity curve

*TTP: time to peak

* Δ ADC: ADC_(lesion) - ADC_(lymphadenopathy). Abbreviations: KD: Kimura's disease, SS&MALT: Sjogren's syndrome with mucosa-associated lymphoid tissue lymphoma, NF: neurofibromatosis

lymphadenopathy often exhibited iso- and hyper-intensity signals, respectively, but their enhancement patterns differed significantly. While 93.5% of primary KD lesions showed heterogeneous enhancement, all lymphadenopathy exhibited homogeneous enhancement. Additionally, skin thickening, found in 72.2% of cases, would be a notable feature of KD, often caused by chronic inflammation and subcutaneous tissue proliferation.

Functional MRI findings

Functional MRI, including DWI and DCE-MRI, offers promising markers like the ADCs and TIC patterns, which can distinguish between head and neck diseases [29–31]. Our study, which included both ADC and TIC data, is the largest series of KD cases reported to date. The significant differences in ADCs (Δ ADC) between primary lesions and lymphadenopathy were especially interesting, as they could provide a non-invasive marker for distinguishing KD from lymphoma. The TIC patterns further supported these findings, with KD lesions showing patterns more akin to NF and lymphoma exhibiting a broader variety of patterns. Δ ADC and TIC patterns between primary lesions and lymphadenopathy may be attributed to variations in tissue composition. Subcutaneous lesions often have more fibrotic tissue, leading to higher ADCs and a progressive enhancement pattern on DCE-MRI. Lymphadenopathy, however, typically showed

lower ADCs due to its hypercellular nature [14]. This observation has also been noted by Horikoshi et al. [14] and may be a distinctive feature of KD.

Stepwise decision tree model for differential diagnosis of KD

To improve diagnostic accuracy, we utilized a stepwise decision-tree model, which is advantageous over traditional logistic regression. CART selected the most significant variables and excluded irrelevant ones, making it particularly effective for small sample sizes. As shown in Fig. 6, ADCs emerged as the most discriminative feature, allowing differentiation between KD and conditions like lymphoma, NF and SS&MALT. KD with lower ADCs ($\leq 0.83 \times 10^{-3}$ mm²/s) could be easily misled to lymphoma. However, it could be further differentiated by examining the maximum diameter of the lymphadenopathy. Similarly, KD with ADCs greater than 0.83×10^{-3} mm²/s and no lymphadenopathy might be confused with NF, but this distinction could be made by using a higher ADC cutoff of 1.2×10^{-3} mm²/s. Typically, KD showed ADCs between 0.83×10^{-3} mm²/s and 1.2×10^{-3} mm²/s, whereas NF ADCs were usually higher than 1.2×10^{-3} mm²/s. Overall, the decision tree model demonstrated excellent accuracy in distinguishing KD from other conditions such as SS&MALT. This model offered several advantages over traditional methods. For example, the

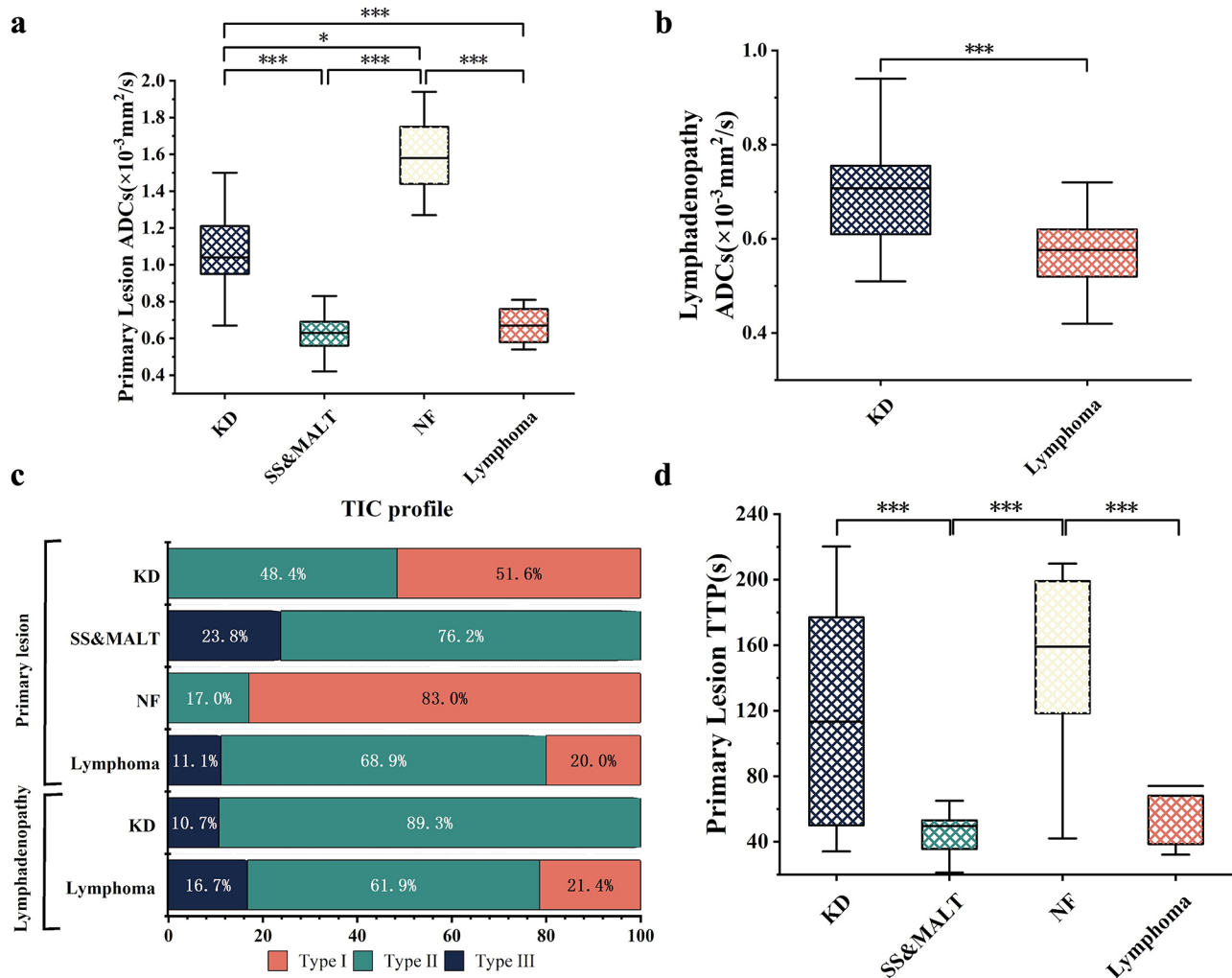


Fig. 5 Comparison of parameters derived from DWI and DCE-MRI in KD and three other head and neck conditions. **(a)** ADCs of primary lesions across four conditions. **(b)** ADCs of lymphadenopathy in KD and lymphoma. **(c)** TIC patterns of lesions and lymphadenopathy across four conditions illustrated distinct dynamic enhancement characteristics. **(d)** TTP values of primary lesions across four conditions highlighted differences in enhancement kinetics. Statistical analysis was performed using Kruskal-Wallis H test, Mann-Whitney U test, Chi-square test, and Fisher's exact test. Significantly different P values at $P < 0.05$ (*) or $P < 0.001$ (***) . *Abbreviations:* ADC, apparent diffusion coefficient; KD, Kimura's disease; SS&MALT, Sjogren's syndrome with mucosa-associated lymphoid tissue lymphoma; NF, neurofibromatosis; TIC, time-signal intensity curve; TTP, time to peak

decision-making process was quick and automated by analysing key parameters such as ADCs, lesions sizes and locations, particularly for diseases with nonspecific imaging findings or when we are less familiar with the condition. Additionally, this model can potentially guide management decisions. For example, distinguishing KD from lymphoma could avoid unnecessary treatments, such as chemotherapy or radiation therapy. By accurately diagnosing KD, the model would help direct more appropriate interventions, such as corticosteroids or immunosuppressive therapy. This personalized approach can lead to better patient outcomes, with a reduced risk of adverse effects from inappropriate treatments.

Limitations and future directions

Our study still had some limitations. The small sample size, due to the rarity of KD, resulted in a limited number of cases for analysis. Additionally, misclassification occurred in two KD cases—one was incorrectly identified as lymphoma due to a markable enlarged lymph node (up to 6 cm), and the other, involving both the lacrimal gland and adjacent soft tissues, was misclassified as NF due to a higher ADC value resulting from the soft tissue involvement. These misclassifications highlighted the challenges in differentiating KD from lymphoma or NF when larger lymph nodes or lesions involving soft tissues were present. Future studies with larger cohorts and more detailed imaging and clinical metrics will help further refine the decision tree model. Incorporating additional imaging

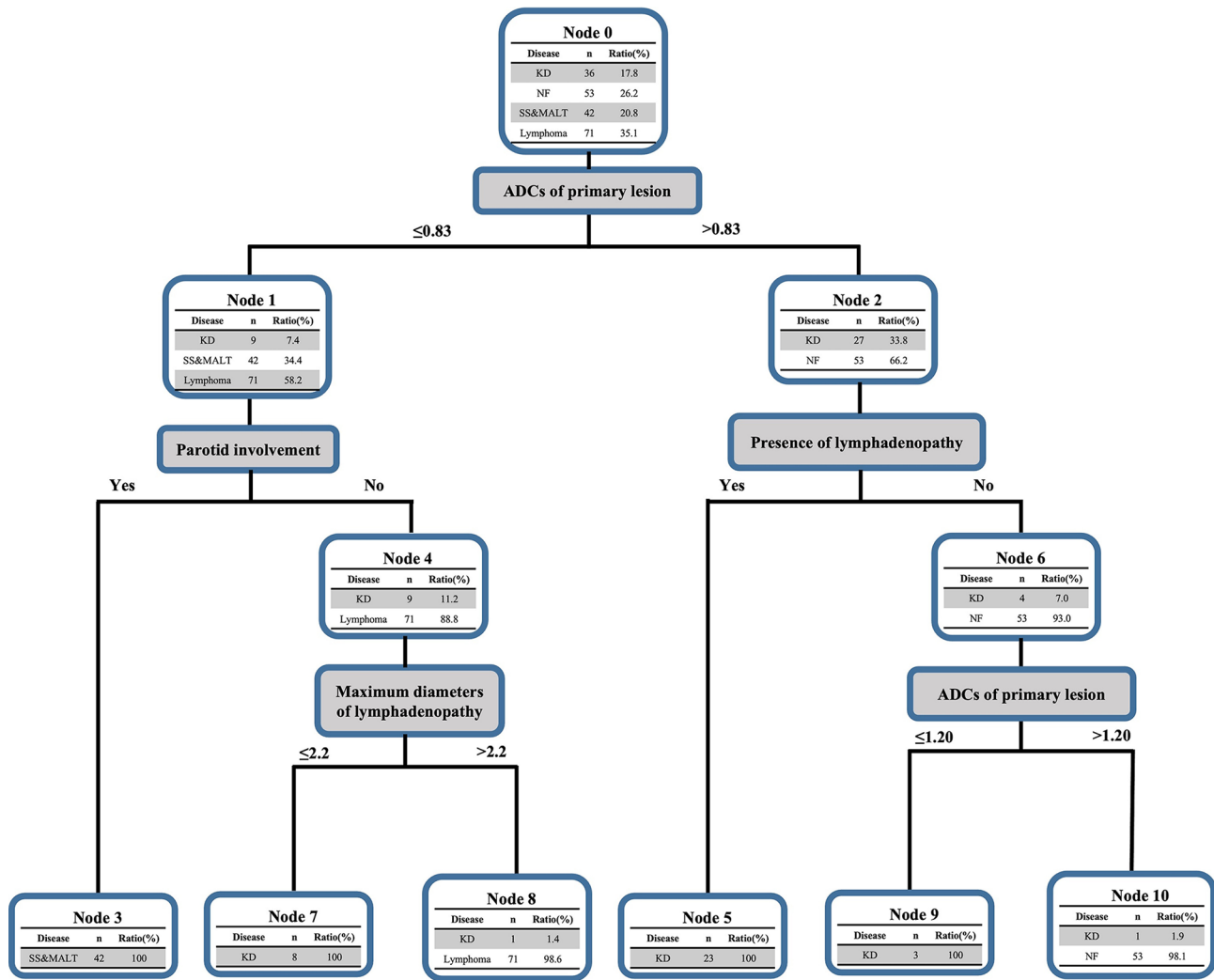


Fig. 6 Stepwise approach for discrimination of KD and three other head and neck conditions. The decision tree model illustrated a structured approach for distinguishing KD from SS&MALT, NF, and primary lymphoma based on routine and functional imaging features. The initial split was based on an ADC threshold of $0.83 \times 10^{-3} \text{ mm}^2/\text{s}$, effectively categorizing 202 cases. Left Panel: For cases with lower ADCs ($\leq 0.83 \times 10^{-3} \text{ mm}^2/\text{s}$), parotid gland involvement served as a distinguishing feature, achieving 100% accuracy in identifying SS&MALT. In cases with no parotid involvement, a lymphadenopathy maximum diameter threshold of 2.2 cm differentiated KD (diameter ≤ 2.2 cm) from primary lymphoma (diameter > 2.2 cm) with high accuracy (100% for KD and 98.4% for lymphoma). Right Panel: For cases with higher ADCs ($> 0.83 \times 10^{-3} \text{ mm}^2/\text{s}$), the presence of lymphadenopathy indicated KD with 100% accuracy. In the absence of lymphadenopathy, KD and NF were further differentiated by an ADC threshold of $1.2 \times 10^{-3} \text{ mm}^2/\text{s}$, achieving 100% accuracy for KD (ADCs $\leq 1.2 \times 10^{-3} \text{ mm}^2/\text{s}$) and 98.1% for NF (ADCs $> 1.2 \times 10^{-3} \text{ mm}^2/\text{s}$). Overall, the decision tree model attained a 99.0% accuracy rate in distinguishing these four diseases, with a misclassification risk of 0.079 ± 0.024 as validated by 10-fold cross-validation. *Abbreviations:* ADC, apparent diffusion coefficient; KD, Kimura’s disease; SS&MALT, Sjogren’s syndrome with mucosa-associated lymphoid tissue lymphoma; NF, neurofibromatosis

parameters and expanding the sample size will enhance its accuracy, potentially making it a standard tool in clinical practice for diagnosing KD and similar diseases. Once trained, the model could be seamlessly integrated into clinical settings with minimal additional cost, relying on data already collected from routine imaging studies.

Conclusion

In conclusion, the stepwise decision tree model, incorporating both routine and functional MRI features, showed high accuracy in differentiating KD from other head and

neck conditions, offering a reliable diagnostic tool for radiologists and physicians in daily practice and guiding tailored clinical management plans for affected patients.

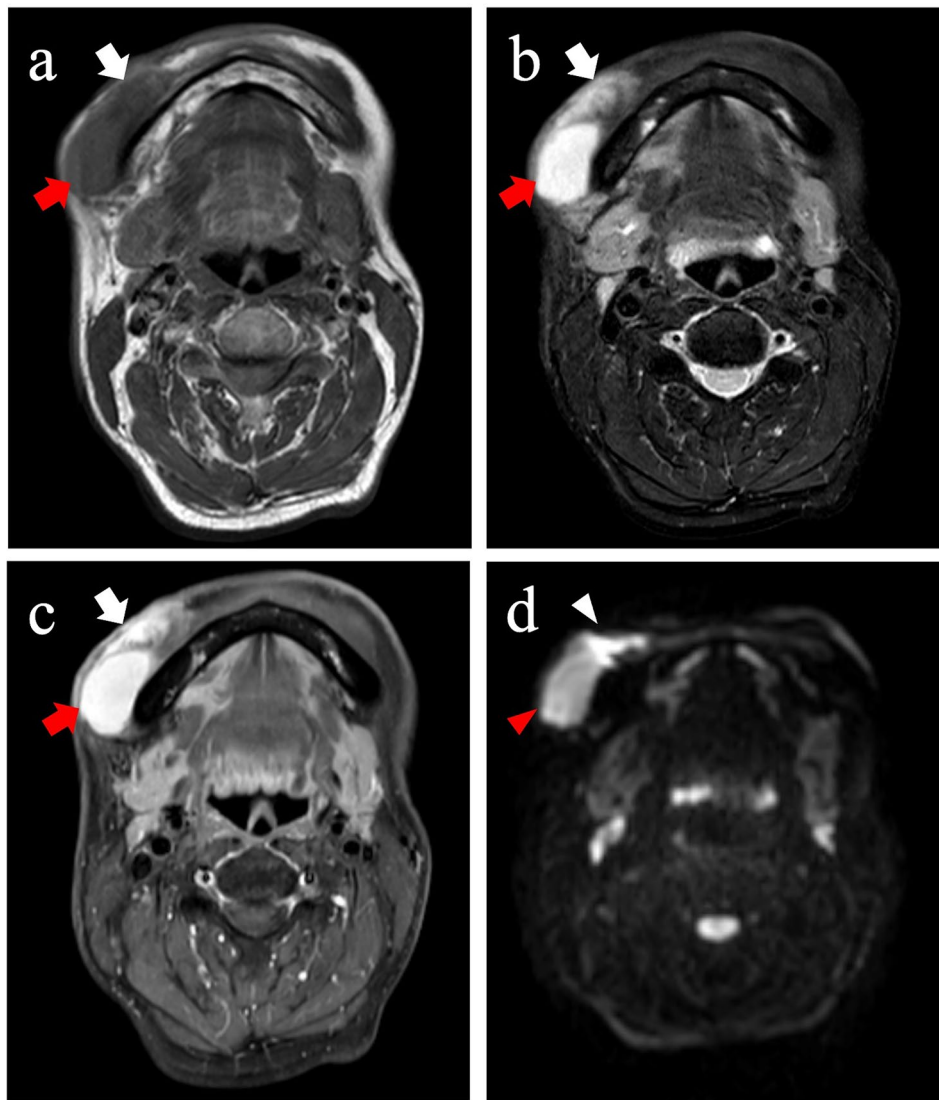


Fig. 7 A well-defined nodular and an ill-defined infiltrative pattern coexisted in one KD case. **(a, b)** Axial T1WI and fat-suppressed T2WI revealed an ill-defined infiltrative lesion (white arrow) and a well-defined nodular lesion (red arrow) as well. **(c)** On axial fat-suppressed contrast-enhanced T1WI, the infiltrative lesion (white arrow) showed heterogeneous and remarkable enhancement, while the nodular lesion (red arrow) exhibited homogeneous, marked enhancement. **(d)** DWI showed the infiltrative lesion (white arrowhead) and the nodular lesion (red arrowhead)

Abbreviations

ADC	Apparent diffusion coefficient
CT	Computed tomography
CART	Classification and regression trees
DWI	Diffusion weighted imaging
DCE-MRI	Dynamic contrast-enhanced MRI
KD	Kimura's disease
MRI	Magnetic resonance imaging
NF	Neurofibromatosis
ROI	Regions of interest
SS&MALT	Sjogren's syndrome with mucosa-associated lymphoid tissue lymphoma
TIC	Time-signal intensity curve
TTP	Time to peak
T1WI	T1-weighted imaging
T2WI	T2-weighted imaging

Acknowledgements

Not applicable.

Author contributions

R.L.: Writing—original draft, Methodology, Data collection and analysis. G.X.Y.: Data collection and analysis. Z.T.: Pathological evaluation, Writing-review & editing. Y.N.H.: Statistical analysis, Methodology. Y.S.H.: Writing-review & editing. H.M.S.: Methodology, Writing-review & editing. Y.W.W.: Conceptualization, Writing—original draft, Writing-review & editing, Supervision, Project administration.

Funding

This study has received funding by the National Natural Science Foundation of China (Grant No. 82373114 to YW Wu) and Cross Disciplinary Research Fund of Shanghai Ninth People's Hospital, Shanghai Jiao Tong University, School of Medicine (No. JYJC202107 to YW Wu).

Data availability

The datasets generated and analysed during the current study are not publicly available due to the hospital policy but are available from the corresponding author on reasonable request.

Declarations

Ethics approval and consent to participate

This study was approved by the Medical Ethics Committee of Shanghai Ninth People's Hospital, Shanghai Jiao Tong University School of Medicine (No. SH9H-2024-T168-1). All protocols were carried out by following the guidelines of Declaration of Helsinki. All participants or their guardians were informed of the specific details of the study and signed the informed consents before enrollment.

Consent for publication

Not applicable.

Competing interests

The authors declare no competing interests.

Author details

¹Department of Radiology, Shanghai Ninth People's Hospital Affiliated to Shanghai Jiao Tong University School of Medicine, Shanghai 200011, China

²Department of Statistics, Shanghai Ninth People's Hospital Affiliated to Shanghai Jiao Tong University School of Medicine, Shanghai 200011, China

³Department of Oral Pathology, Shanghai Ninth People's Hospital Affiliated to Shanghai Jiao Tong University School of Medicine, Shanghai 200011, China

Received: 3 December 2024 / Accepted: 25 February 2025

Published online: 17 March 2025

References

1. Stuczyński SK, Muras-Szwedziak K, Nowicki M. Wyzwania w diagnostyce choroby Kimury [Diagnostic challenges in Kimura's disease]. *Polski Merkurusz Lekarski: Organ Polskiego Towarzystwa Lekarskiego*. 2022;50(296):128–30.
2. HT K. Eosinophilic hyperplastic lymphogranuloma, comparison with Mikulicz's disease. *Chin Med J*. 1937;23:699–670.
3. Kimura T, Yoshimura S, Ishikawa E. Unusual granulation combined with hyperplastic changes of lymphatic tissue. *Trans Soc Pathol*. 1948;37:179–80.
4. Park SW, Kim HJ, Sung KJ, Lee JH, Park IS. Kimura disease: CT and MR imaging findings. *AJNR Am J Neuroradiol*. 2012;33(4):784–8.
5. Zhu WX, Zhang YY, Sun ZP, Gao Y, Chen Y, Yu GY. Differential diagnosis of Immunoglobulin G4-related sialadenitis and Kimura's disease of the salivary gland: a comparative case series. *Int J Oral Maxillofac Surg*. 2021;50(7):895–905.
6. Lee CC, Feng JJ, Chen YT, Weng SF, Chan LP, Lai CS, Lin SD, Kuo YR. Treatment algorithm for Kimura's disease: A systematic review and meta-analysis of treatment modalities and prognostic predictors. *Int J Surg (London England)*. 2022;100:106591.
7. Lee CC, Yu KH, Chan TM. Kimura's disease: A clinicopathological study of 23 cases. *Front Med*. 2022;9:1069102.
8. Zhang G, Li X, Sun G, Cao Y, Gao N, Qi W. Clinical analysis of Kimura's disease in 24 cases from China. *BMC Surg*. 2020;20(1):1.
9. Kakehi E, Kotani K, Otsuka Y, Fukuyasu Y, Hashimoto Y, Sakurai S, Hirotsu A, Simizu K, Fujita R, Shoji K, Adachi S, Matsumura M. Kimura's disease: effects of age on clinical presentation. *QJM: Monthly J Association Physicians*. 2020;113(5):336–45.
10. Hashida Y, Higuchi T, Nakajima K, Ujihara T, Murakami I, Fujieda M, Sano S, Daibata M. Human polyomavirus 6 with the Asian-Japanese genotype in cases of Kimura disease and angiolymphoid hyperplasia with eosinophilia. *J Invest Dermatol*. 2020;140(8):1650–e16534.
11. King RL, Tan B, Craig FE, George TI, Horny HP, Kelemen K, Orazi A, Reichard KK, Rimsza LM, Wang SA, Zamo A, Quintanilla-Martinez L. Reactive eosinophil proliferations in tissue and the lymphocytic variant of hypereosinophilic syndrome. *Am J Clin Pathol*. 2021;155(2):211–38.
12. Sato R, Bandoh N, Goto T, Ichikawa H, Uemura A, Suzuki S, Yamaguchi T, Aimonio E, Nishihara H, Katada A, Harabuchi Y. Kimura disease presenting with buccal mass: A case report and literature review. *Head Neck Pathol*. 2021;15(2):657–62.
13. Gopinathan A, Tan TY. Kimura's disease: imaging patterns on computed tomography. *Clin Radiol*. 2009;64(10):994–9.
14. Horikoshi T, Motoori K, Ueda T, Shimofusa R, Hanazawa T, Okamoto Y, Ito H. Head and neck MRI of Kimura disease. *Br J Radiol*. 2011;84(1005):800–4.
15. Sangwan A, Goyal A, Bhalla AS, Kumar A, Sharma R, Arava S, Dawar R. Kimura disease: A case series and systematic review of Clinico-radiological features. *Curr Probl Diagn Radiol*. 2022;51(1):130–42.
16. Wang J, Tang Z, Feng X, Zeng W, Tang W, Wu L, Jin L. Preliminary study of diffusion-weighted imaging and magnetic resonance spectroscopy imaging in Kimura disease. *J Craniofac Surg*. 2014;25(6):2147–51.
17. Povlow MR, Streiff M, Madireddi S, Jaramillo C. (2021). A primary Parotid Mucosa-Associated lymphoid tissue Non-Hodgkin lymphoma in a patient with Sjogren syndrome. *Cureus*. 13(6): e15679.
18. Tonami H, Matoba M, Yokota H, Higashi K, Yamamoto I, Sugai S. Mucosa-associated lymphoid tissue lymphoma in Sjogren's syndrome: initial and follow-up imaging features. *AJR Am J Roentgenol*. 2002;179(2):485–9.
19. Kwok HM, Ng FH, Chau CM, Lam SY, Ma JK F. Multimodality imaging of extranodal lymphoma in the head and neck. *Clin Radiol*. 2022;77(8):e549–59.
20. Thakur U, Ramachandran S, Mazal AT, Cheng J, Le L, Chhabra A. Multiparametric whole-body MRI of patients with neurofibromatosis type I: spectrum of imaging findings. *Skeletal Radiol*. 2025;54(3):407–22.
21. Han MM, Dermakarian CR, Valle Estopinal D, M. D., Tao JP. Kimura disease of the periorbital and earlobe in a 15-Year-Old male: A case report and review of the literature. *Ophthal Plast Reconstr Surg*. 2023;39(1):26–33.
22. Zhang C, Chen J, Hui Y, Chen H, Deng D, Sang H, Liu F. Risk of nephritis and recurrence in Kimura disease: A retrospective study. *Indian J Dermatology*. 2023;68(6):611–8.
23. Arshad AR. Kimura's disease of Parotid gland presenting as solitary Parotid swelling. *Head Neck*. 2003;25(9):754–7.
24. Rovlias A, Kotsou S. Classification and regression tree for prediction of outcome after severe head injury using simple clinical and laboratory variables. *J Neurotrauma*. 2004;21(7):886–93.
25. Li X, Wu X, Qian J, Yuan Y, Wang S, Ye X, Sha Y, Zhang R, Ren H. Differentiation of lacrimal gland tumors using the multi-model MRI: classification and regression tree (CART)-based analysis. *Acta Radiol (Stockholm Sweden)*. 2022;63(7):923–32.
26. Vallée R, Vallée JN, Guillevin C, Lallouette A, Thomas C, Rittano G, Wager M, Guillevin R, Vallée A. Machine learning decision tree models for multiclass classification of common malignant brain tumors using perfusion and spectroscopy MRI data. *Front Oncol*. 2023;13:1089998.
27. Kelly HR, Curtin HD. Chapter 2 squamous cell carcinoma of the head and Neck-Imaging evaluation of regional lymph nodes and implications for management. Volume 38. *Seminars in ultrasound*; 2017. pp. 466–78. 5.
28. Loh W. Fifty years of classification and regression trees. *Int Stat Rev*. 2014;82(3):329–48.
29. Malla SR, Bhalla AS, Manchanda S, Kandasamy D, Kumar R, Agarwal S, Shamim SA, Kakkar A. Dynamic contrast-enhanced magnetic resonance imaging for differentiating head and neck paraganglioma and Schwannoma. *Head Neck*. 2021;43(9):2611–22.
30. Vijayalakshmi K, Raghuram PH, Saravanan K, Krithika CL, Kannan A. Validity of 3-Tesla diffusion-weighted magnetic resonance imaging for distinction of reactive and metastatic lymph nodes in head-and-neck carcinoma. *J Cancer Res Ther*. 2020;16(3):587–93.
31. Xu Z, Zheng S, Pan A, Cheng X, Gao M. A multiparametric analysis based on DCE-MRI to improve the accuracy of Parotid tumor discrimination. *Eur J Nucl Med Mol Imaging*. 2019;46(11):2228–34.

Publisher's note

Springer Nature remains neutral with regard to jurisdictional claims in published maps and institutional affiliations.